Plasma Dynamics and Pulse Shape Rules in Laser Heating of Opaque Targets in Air

Bassam Hanna Habib

Al-Mansour University College

Abstract

A theoretical model is developed to determine time evolution of temperature at the surface of an opaque target placed in air for cases characterized by the formation of laser supported absorption waves (LSAW) plasmas. The model takes into account both plasma dynamics and time variation of incident laser pulse (i.e. pulse shape or profile).Shock tube relations were employed in formulating plasma dynamics over target surface. Gaussian function was chosen in formulating the pulse profile in the present modeling.

Keywords

Plasma Dynamics
Laser Heating

Article info
Received: Mar. 2010
Accepted: Apr. 2010
Published: Nov. 2010

تأثير ديناميكية البلازما و شكل النبضة في التسخين الليزري للأهداف المعتمة في الهواء

د. بسام حنا حبيب
كلية المنصور الجامعة

الخلاصة

تم تطوير نموذج نظري لأحتساب التغير الزمني للحرارة عند اسطح الأجسام المعتمة في الهواء للحالات المصاحبة بتولد بلازما الأمتصاص المعززة بالليزر(LSAW). يأخذ النموذج الحالي في الحسبان كل من ديناميكية البلازما و التغير الزمني للنبضة الليزرية (شكل النبضة). تم استخدام بعض معادلات انبوبة موجة العصف (Shock Tube Relations) في نمذجة ديناميكية البلازما عند سطح الهدف. تم اعتماد الدالة الكاوسية لصياغة النبضة الليزرية في النمذجة الحالية.

Introduction

Interaction of high intensity laser beams with solid targets accompanied by the generation of plasmas has received considerable attention in applications like spectroscopy [1], industry as well as military [2].

Characteristics of such plasmas depend largely on experimental parameters like laser beam intensity; laser pulse duration and shape (for pulsed lasers) [3], target surface condition and thermal properties [4].

In particular, for solid targets placed in air under atmospheric pressure, and for proper laser beam intensities, Laser Supported Absorption (LSA) waves (or LSAW) plasmas may be generated adjacent to the target front surface [5]. Once LSA plasma is generated it is heated by absorbing laser beam energy. As a result, the heated plasma expands rapidly over the target surface and propagates into the ambient air both radially over the target surface and axially away from the surface toward the laser source. The LAS plasma expansion mechanism resembles that of spherical blast propagation as illustrated schematically in Fig. (1) [6].

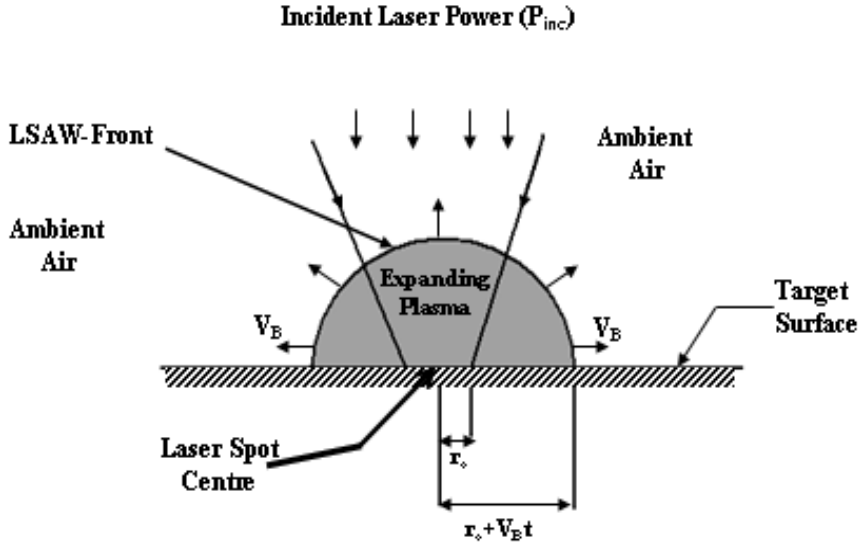

Fig.(1)

A scheme represents the expansion of LSA plasma over target surface in air.

LSA plasmas act to enhance the heat coupling coefficient (i.e. fraction of laser energy absorbed by the target). This enhancement is achieved by both uv radiation emitted from the plasma, and thermal conduction across the plasma/target interface while the LASW is in contact with the target surface [6].

On the other hand, lateral expansion of LSAW over the target surface causes the target/plasma interface area to increase {Fig. (1)}, accordingly the energy flux density transferred to target surface from the plasma will be decreased since the incoming energy will be distributed over an increasing area. This retards the heating rate of the target [6].

Hence it may be stated that the incoming energy flux from the plasma tend to increase the surface heating while energy spreading over the surface due to plasma lateral expansion as well as heat flow from the surface into the target bulk via thermal conduction tend to retard surface heating.

Theoretical Aspects

Referring to fig. (1), plasma- target interface area A(t) increases with time due to lateral expansion of the generated plasma in the form [6]:

$$A(t) = \pi (r_o + V_B t)^2 \quad \ldots\ldots\ldots\ldots (1)$$

where r_o: laser spot radius and V_B: LSAW-lateral blast velocity and t is the time. Consequently, the on- target power density [I(t)] may be effectively defined as [6]:

$$I(t) = \mu_{eff} P_{inc}(t) / A(t) \quad \ldots\ldots\ldots\ldots (2)$$

where μ_{eff} : effective coupling coefficient, and P_{inc} (t): incident laser power.

The coupling coefficient factor (μ_{eff}) reaches maximum values (~ 0.15 – 0.3) for incident laser power density in the range (1 -2) x10^6 W/cm^2 [6].

For a semi- infinite solid target at an initial uniform temperature (Ti) subjected to an incident heat flux [I(t)], the surface-temperature behavior is given as [6]:

$$\Delta T(t) = T(t) - Ti = \frac{k^{1/2}}{K\pi^{1/2}} \int_0^t \frac{I(t-t')}{t'^{1/2}} dt'$$

…… (3)

where t′ varies from o to t, T(t) and ΔT(t) are surface instantaneous temperature and temperature change respectively; k and K

are thermal diffusivity and conductivity of target material respectively. Using eqs. (1) and (2) with the approximation of a constant laser power (Pc) throughout a pulse duration (i.e. a rectangular pulse), and a constant (average) blast wave velocity (V_B), eq.(3) may be written in the form [6]:

$$\Delta T(\xi) = \frac{\mu_{eff} P_c k^{1/2}}{K(\pi\tau_p)^{3/2}} \int_0^{\xi} \frac{d\xi'}{(\xi')^{1/2}[r_o/\tau_p + V_B \times (\xi - \xi')]^2} \quad \ldots\ldots\ldots\ldots\ldots\ldots (4)$$

where ξ is a normalized time factor ($\xi = t/\tau_p$). Equation (4) may be integrated analytically to yield surface temperature (T) at any instant (ξ) throughout an incident laser pulse duration [6], where: $T(\xi) = Ti + \Delta T(\xi)$, with (Ti) as an initial surface temperature.

Present Modeling Features

In the present model, time dependence of both laser power (P_{inc}) and plasma lateral velocity (V_B) are taken into account. This makes it unavoidable to solve the integral in eq.(3) numerically.

1. Time Dependence of Laser Power

It is more convenient to describe incident laser power [$P_{inc}(t)$] in terms of power density [I(t)] among laser spot area (A_o) since LSAW ignition condition is specified conventionally via power density factor [5], hence we may write:

$$P_{inc}(t) = I(t) \,.\, A_o \quad \ldots\ldots\ldots\ldots (5)$$

Using eqs.(1), (2) and (5), equation (3) may be written in terms of normalized time as:

$$\Delta T(\xi) = \frac{k^{1/2} \mu_{eff} A_o}{K(\tau_p \pi)^{3/2}} \int_0^{\xi} \frac{I(\xi - \xi')}{\xi'^{1/2}[\frac{r_o}{\tau_p} + V_B(\xi - \xi') \times (\xi - \xi')]^2} d\xi' \quad \ldots\ldots\ldots\ldots\ldots (6)$$

Pulse shape (or profile) is introduced via mathematical expressions chosen for power density (I) in the integrand of eq.(6).

A Gaussian pulse is adopted in this work of a form given as:

$$I(t) = A_P e^{-\mu(t_o - t)^2} \,,$$

with $t_o = \tau_p/2$, and μ is a constant to be formulated.

As an approximation for facilitating calculations, only a portion of the whole pulse is considered, which guarantees the existence of an LSAW with an appreciable coupling coefficient (μ_{eff}). This portion is shown in Fig.(2) as a shaded part of the whole profile.

To formulate this portion of the power density which lies between a lower level (B_P) and an upper level (A_P), the factor (μ) in the Gaussian form of the pulse should take the form: $\mu = 4 \ln(A_P/B_P)/\tau_p^2$.

From Fig.(2) it may be stated that the laser pulse incident on the target is assumed as a selected portion of the Gaussian profile that exceeds a lower level (B_P) of a duration (τ_p).

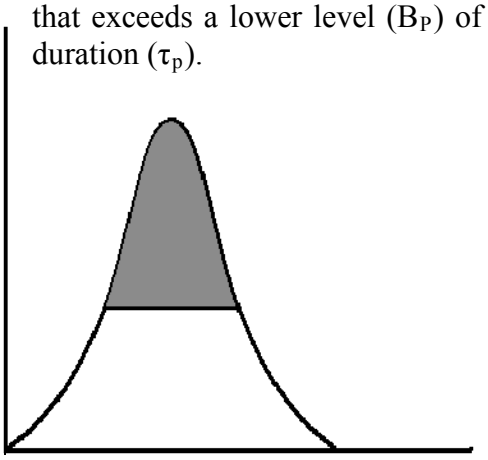

Fig.(2) Schematic representation of pulse profile employed in the present calculations

2. Time Dependence of Plasma Lateral Velocity

Plasma lateral blast wave velocity (V_B) depends on incident laser power magnitude and hydrodynamic condition of expanding plasma over target surface [5]. Plasma status above target surface is illustrated in Fig.(3) as a top view of the situation shown in Fig.(1).

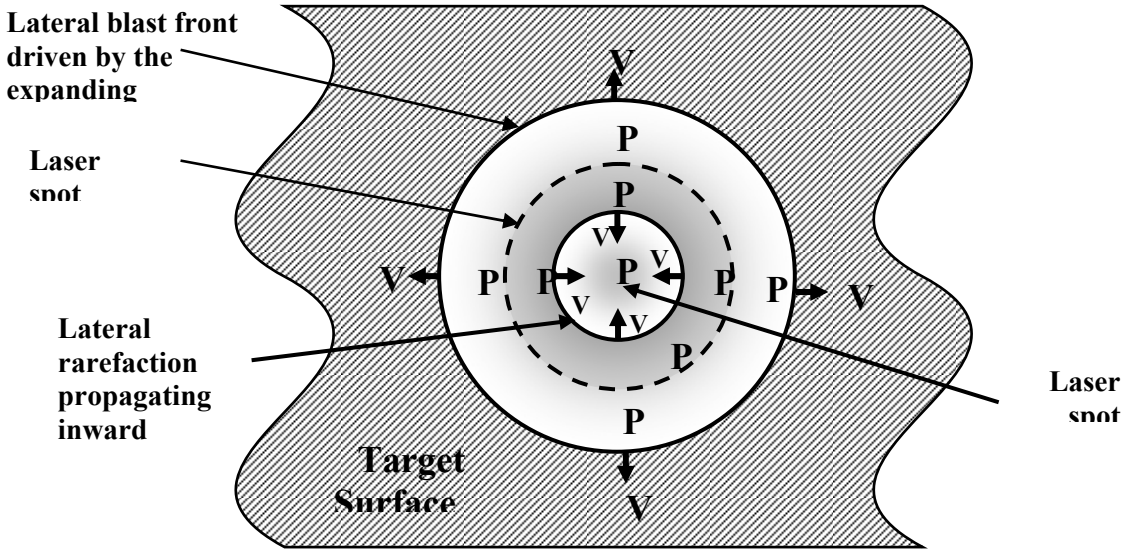

Fig.(3): A top view of plasma status over target surfac

As indicated in Fig.(3), Plasma pressure (P_L) drives the lateral blast wave which propagates outward over target surface with velocity (V_B) that depends on instantaneous values of incident laser energy. A cylindrical rarefaction propagates laterally inward throughout the plasma towards laser spot centre with velocity (V_S) causing plasma pressure relaxation from a higher value (P_H) to a lower one (P_L). Once this rarefaction reaches the spot centre, two dimensional effects start to influence the hydrodynamics of the expanding plasma causing the blast wave velocity (V_B) to decrease with time.
Effects of laser power- and plasma dynamics on lateral blast velocity (V_B) are described in the following two paragraphs.

2.1 Influence of Laser Power on V_B Blast wave velocity may be determined from its Mach number (M) as [7]:
$V_B = M * a$ …… (7),

Where (a) is sound speed in ambient air. Using shock tube relations, the Mach number may be formulated as [8]:

$$M = [\frac{(\gamma_o + 1) \times (P_L / P_o) + \gamma_o - 1}{2\gamma_o}]^{1/2}$$

…….. (8)

where γ_o and P_o are respectively the specific heat ratio and pressure of ambient air, and P_L is the plasma pressure just behind the blast wave front, it is the driving pressure of the lateral blast [Fig.(3)] and may be obtained by numerically solving the equation [5]:

$$(\frac{\gamma_o P_o}{\rho_o})^{1/2} (\frac{P_L}{P_o} - 1)[\frac{2/\gamma_o}{(\gamma_o + 1)P_L / P_o + \gamma_o - 1}]^{1/2} = \frac{2V_s}{\gamma - 1}[1 - (P_L / P_H)^{\frac{\gamma - 1}{2\gamma}}]$$

…. (9)

here ρ_o is the ambient air density, γ is the plasma specific heat ratio, V_S is the inward rarefaction velocity, and P_H represents plasma pressure in front of the rarefaction wave that relaxes to the lower value P_L (blast driving pressure) [fig.(3)].
The velocity V_S and pressure P_H are given as [5]:

$$V_S = (\frac{\gamma P_H}{\rho_o})^{1/2}[\frac{W+1}{W}\frac{\gamma_o - 1}{\gamma_o + 1}]^{1/2}$$

…… (10)

$$P_H = (1-\frac{2W}{\gamma_o - 1})(\frac{\gamma_o + 1}{2}\rho_o)^{1/3}$$

$$[\frac{(\gamma-1)(\gamma+1)I(t)}{(\gamma+W)(\gamma_o - 2W - 1)}]^{2/3}$$

….. (11)

where W is a non-dimensional plasma particle velocity relative to LSAW front (taken as 0.04) [5]. So far it can be noticed that both velocities V_B and V_S are time dependent since the incident power density I(t) in eq.(11) is a time dependent quantity.

2.2 Influence of Two- dimensional Plasma Flow on V_B

Referring to Fig(3), when the inward rarefaction reaches laser spot centre, two dimensional plasma flow initiates and begins to affect the plasma dynamics behind the blast front [9] , consequently, blast wave velocity (V_B) will be further affected (decreases with time). It is necessary to specify the instant (τ_D) at which this two dimensional flow begins.

In the present attempt, τ_D is specified by determining successive locations of the inward lateral rarefaction as time goes on, hence τ_D is the instant at which rarefaction front reaches laser spot centre.

After the instant τ_D, two dimensional plasma flow causes plasma pressure (P_L) to decrease with time (decays) causing plasma lateral velocity (V_B) to decrease as well. The decrease in V_B is formulated by making use of a scaling law equation that describes expansion of explosive gases in spherical geometry given as [10]:

$P = P_{ref} (t / t_{ref})$ …….. (12)

where (P) and (t) refer to instantaneous pressure of expanding gases and time respectively, (P_{ref}) refers to gas pressure at a given reference time (t_{ref}). By examining eqs.(7) and (8), a square proportionality may be noticed between blast driving pressure (P_L) and velocity (V_B), hence a scaling low for blast velocity may be deduced from eq.(12) with τ_D as a reference time in the form:

$V_B = V_B(\tau_D)\ (t/\tau_D)$, $t > \tau_D$ …… (13)

3. Present Model Calculations

The time τ_D is firstly determined by tracing the rarefaction front as it proceeds toward the spot centre [Fig.(3)]. This is done by determination of the velocity (V_S) after each time step (time increment) Δt using eqs.(10) and (11). This is accompanied with the determination of instantaneous power density [I(t)] in eq.(11) from the proposed Gaussian profile. Time τ_D is assigned when rarefaction front reaches spot centre, a numerical interpolation process is required to get a more precise evaluation of the instant τ_D. Lateral blast velocity at the instant τ_D [$V_B(\tau_D)$] is also determined through eqs.(7)-(11). Determination of τ_D and $V_B(\tau_D)$ makes it possible to employ eq.(13) when it is required. To monitor the surface temperature throughout a single laser pulse duration, the integration of eq.(6) is evaluated for successive increasing upper limits (ξ) until reaching ξ=1 at the termination of the pulse.

Numerical approach is employed in integrating eq.(6) with a normalized time step $\Delta\xi$.

Equations (7)-(11) are used to determine the blast velocity (V_B) when the time is less than (τ_D), and eq.(13) is used when the time exceeds (τ_D).

Procedure of the present calculations may be summarized by the following block diagram:

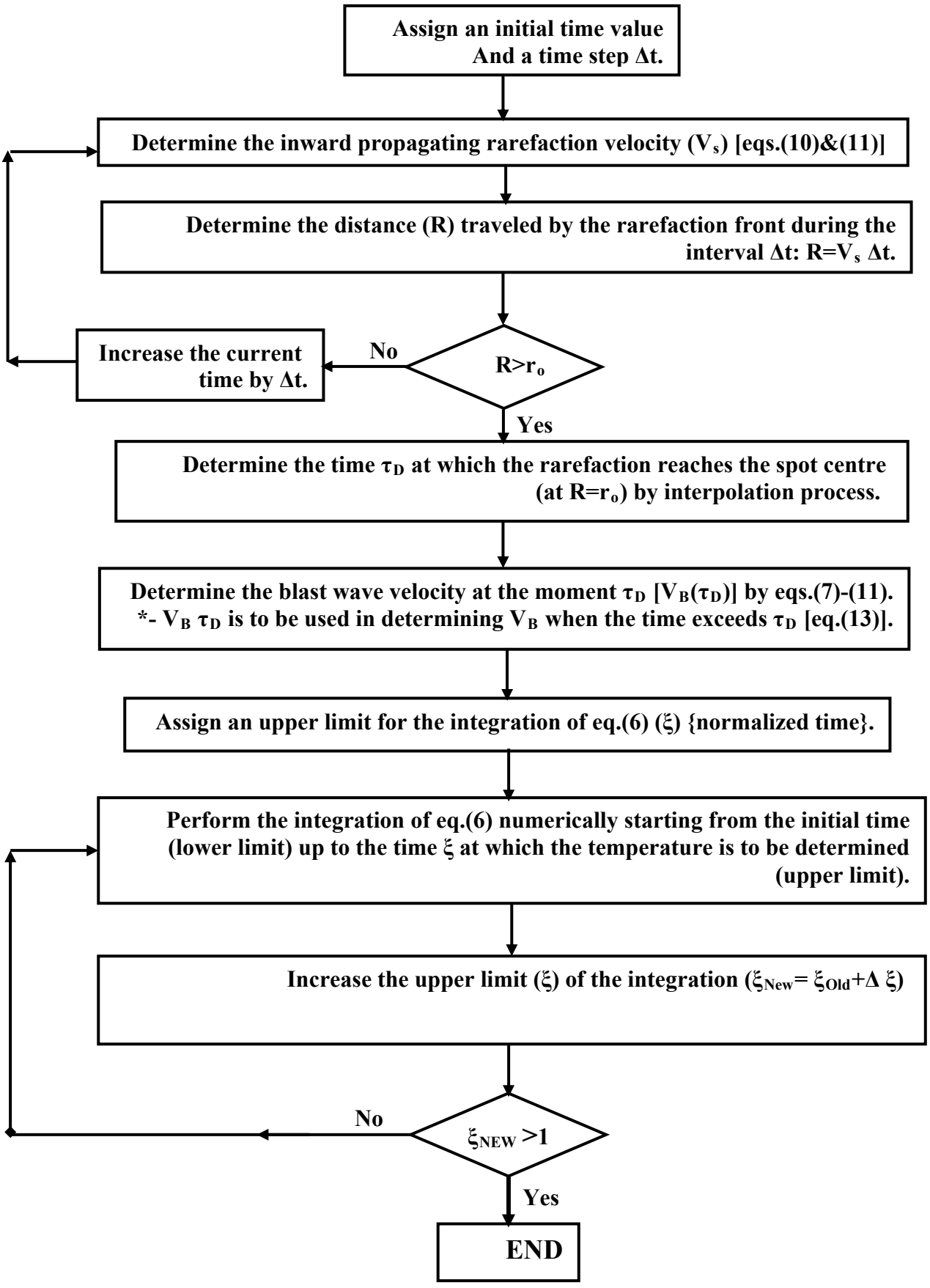
Assign an initial time value And a time step Δt.
Determine the inward propagating rarefaction velocity (V_s) [eqs.(10)&(11)]
Determine the distance (R) traveled by the rarefaction front during the interval Δt: $R=V_s\ \Delta t$.
$R>r_o$
No
Increase the current time by Δt.
Yes
Determine the time τ_D at which the rarefaction reaches the spot centre (at $R=r_o$) by interpolation process.
Determine the blast wave velocity at the moment τ_D [$V_B(\tau_D)$] by eqs.(7)-(11).
*- $V_B\ \tau_D$ is to be used in determining V_B when the time exceeds τ_D [eq.(13)].
Assign an upper limit for the integration of eq.(6) (ξ) {normalized time}.
Perform the integration of eq.(6) numerically starting from the initial time (lower limit) up to the time ξ at which the temperature is to be determined (upper limit).
Increase the upper limit (ξ) of the integration ($\xi_{New}=\xi_{Old}+\Delta\ \xi$)
$\xi_{NEW}>1$
No
Yes
END

Parameters of Ref.[8] are employed in the present calculations (for comparison purpose), namely: laser pulse duration (20 μs), laser spot radius (0.1 cm), effective coupling {μ_{eff}} (0.2) [appeared in eq. (2)], and initial surface temperature (Ti) is assumed zero ($^{\circ}$C).

Upper and lower levels of the proposed Gaussian profile {A_P and B_P respectively in Fig.(2)} are chosen as $A_P=2X10^6$ W/cm^2 and $B_P=10^6$ W/cm^2, these values with $\tau_p=20\mu s$ yield an average power density of approximately $1.6x10^6$ W/cm^2 which fulfills the requirement of high coupling coefficient which was stated to occur at power densities in the range (10^6-$2x10^6$ W/cm^2) [6].

Referring to Fig.(2), and with those chosen values of A_P and B_P , it may be recognized that the level B_P (10^6 W/cm^2) with the duration τ_p may be regarded as the FWHM of the whole pulse.

Results and Discussion

The proposed model is applied here to determine temporal variation of surface temperature for a thick aluminum target placed in air due to a single laser pulse, provided the formation of LSA plasmas.

To examine plasma dynamics effect, figure (4) shows the surface temperature as a function of normalized time (ξ) throughout a laser pulse duration of a rectangular pulse of altitude 10^6 W/cm^2. A comparison is made between a case of a constant blast velocity (V_B=500 m/s) [6] where plasma dynamics are not considered, and other of a variable blast velocity where plasma dynamics behind the blast front are considered. Figure (4) shows that constant V_B yields higher temperatures. However the two curves get closer to each other and intersect as the time approaches the end of the pulse. This may be explained by noting Fig.(5) which illustrates the variable blast velocity throughout a pulse duration {the calculations were performed under the same circumstances of Fig.(4)}. It may be noted that the blast velocity is well above 500 m/s at early moments of the pulse. However, it decreases beyond 500 m/s after the first quarter of the pulse, where it is expected that the rate of expansion of the plasma/target interface area to be reduced, this will slow down the decrease in temperature as manifested by the lower curve of Fig.(4).

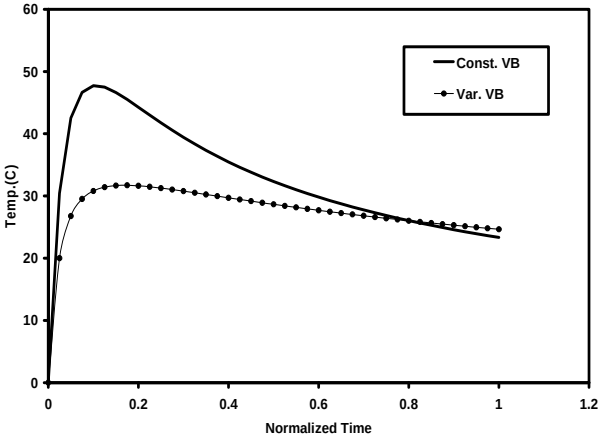

Fig.(4): Surface temperature for constant VB (500m/s) and variable V_B. Laser pulse is assumed rectangular. I=10^6 W/cm^2, τp=20μ_s, Rs=0.1 cm

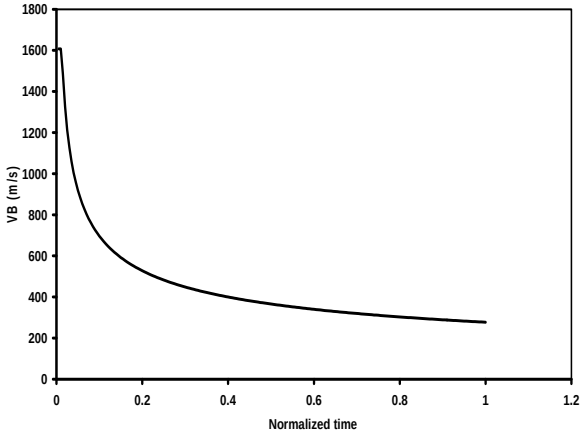

Fig.(5): Blast wave velocity during a rectangular pulse duration. I=10^6 W/cm^2, τp=20μ_s, Rs=0.1 cm.

This may also be confirmed if a comparison is performed concerning plasma/target interface area for the two cases of Fig.(4), which is shown in Fig.(6).

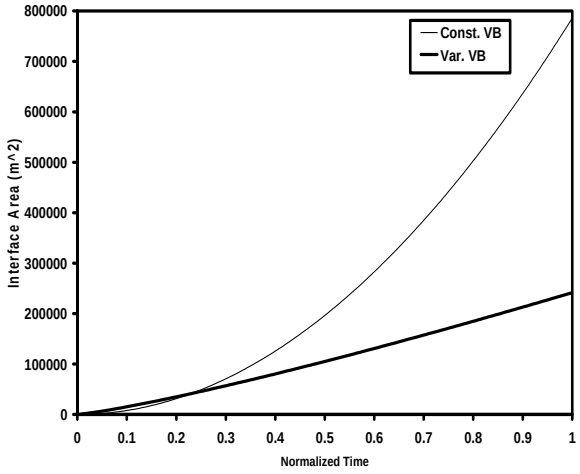

Fig.(6): Plasma/Target interface area increment throughout a rectangular pulse duration for the cases of constant and variables blast velocity.
$I=10^6$ W/cm^2, $\tau p=20\mu_s$, Rs=0.1 cm

As indicated in this figure, the interface area for a constant blast velocity is the lower at the beginning of the pulse causing the relatively high temperatures in Fig.(4), however, at later times during the pulse, this area becomes much higher compared with that of a variable blast velocity {since for a variable V_B condition the two dimensional flow of the plasma acts to reduce it's lateral expansion velocity (V_B)}. Hence the relatively high expansion rate for constant V_B plasma leads to the apparent decrease in surface temperature as indicated in Fig.(4), where due to this high spreading of` power, the heating rate of the surface could not overcome the heat flow from the surface to the target bulk which tends to reduce the surface temperature.

Figure (7) illustrates the effect of laser pulse shape in determining surface temperature, where the blast velocity is assumed constant.

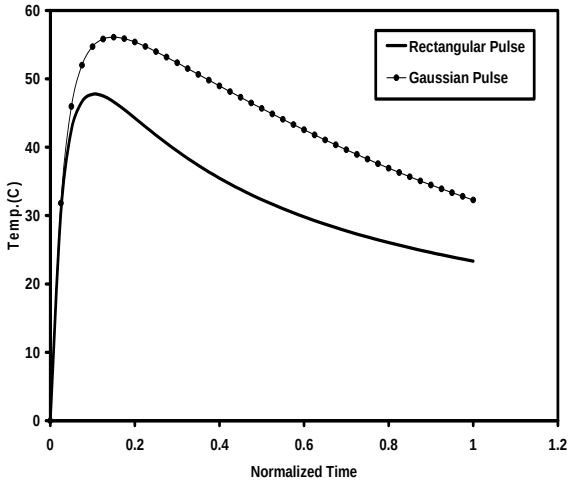

Fig.(7): Surface temperature variation among a laser pulse.
A comparison between rectangular and Gaussian pulses.
V_B=500m/s, $\tau p=20\mu_s$, and Rs=0.1cm for both cases.

Two pulse shapes are examined, a rectangular pulse of altitude 10^6 W/cm^2 and a Gaussian pulse of a lower level B_P= 10^6 W/cm^2 and an upper level A_P= $2x10^6$ W/cm^2 as illustrated in Fig.(2). Influence of the Gaussian pulse is apparent owing to the higher temperatures yielded. However, it may be noted from the trend of the curves in this figure that they tend to approach each other at later times of the pulse, this is due to the drop of the Gaussian profile through its second half.

Influence of both the pulse shape and variations in plasma expansion velocity is shown in Fig.(8) where a comparison is made between a case of rectangular pulse with a constant plasma expansion velocity (V_B) and another case of a Gaussian pulse with a variable V_B.

The same properties regarding power density employed in Fig.(7) are adopted in Fig.(8), a constant V_B of 500m/s is assigned for the rectangular pulse case. The Gaussian pulse shows lower temperatures at the beginning of the pulse duration since the initially determined values of V_B are usually high (compared to the 500m/s) where two dimensional flow

of plasma has not started yet. However, at later times V_B will be reduced gradually, this reduction along with the increase in power density during the first half of the Gaussian pulse profile results in the higher temperatures obtained by the Gaussian pulse curve after the first quarter of the pulse. During the second half of the pulse the Gaussian curve decreases as indicated in Fig.(8). This is due to the decrease in power density for the Gaussian pulse profile during the second half of the duration.

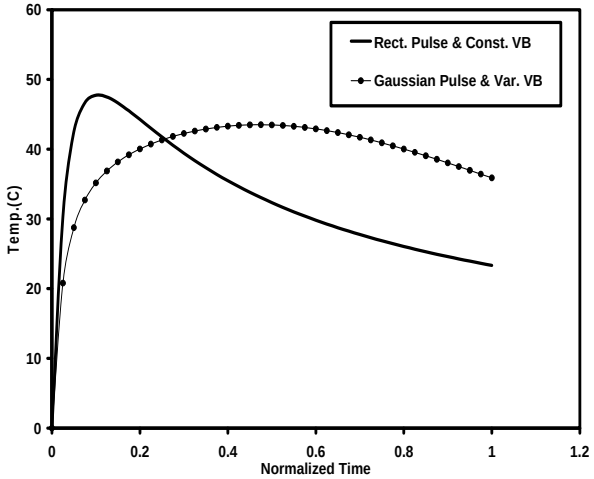

Fig.(8): Surface temperature as a function of time among a laser pulse. A comparison between two cases: a rectangular pulse with a constant V_B and a Gaussian pulse with a variable V_B . ($\tau_p=20\mu_s$, Rs=0.1cm).

Despite this reduction in power density, the final temperature (temperature at the end of the pulse) for the Gaussian pulse (~36 ^oC) is higher compared with that of the rectangular pulse (23 ^oC).

Finally, the effect of laser spot radius (Rs) in heating the target is depicted in Fig.(9), which shows two surface temperature curves one for Rs=0.1cm and the other for Rs=0.5cm. Identical Gaussian power density pulses are assumed for the two cases. As expected the temperatures are higher for the higher radius, this is partly due to increasing power for the larger radius and partly due to the longer delay of the two dimensional plasma flow (τ_D) for the larger radius.

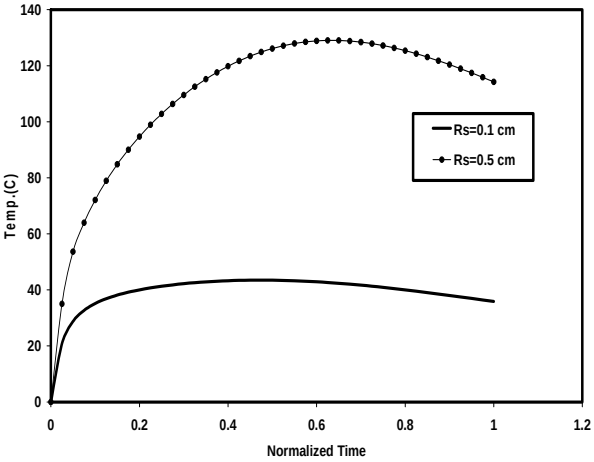

Fig.(9): Influence of laser spot radius in heating the target surface. Identical Gaussian pulses are assumed for the two cases ($B_P=10^6$ W/cm^2 and $A_P=2x10^6$ W/cm^2).

References

[1] Annemie Bogaerts, Zhaoyang Chen: Spectrochimica Acta Part B 60, **(2005)**, 1280-1307.

[2] E. Sturmer, and M von Allmen: J. Appl. Phys.49 (11) , **(1978)**, 5648-5654.

[3] Shannon Mark A., Rostami Ali A. and Russo Richard E., **(1992).** Photo thermal deflection measurements for monitoring heat transfer during modulated laser heating of solids, J. Appl. Phys. 71(1): 53-63.

[4] nnemie Bogaerts, Zhaoyang Chen, Renaat Gijbels, Akos Vertes: Spectrochimica, Acta Part B 58 **(2003)**, 1867-1893

[5] J. P. Reilly, A Balllantyne, and J. A. Woodsoffe: AIAA JOURNAL 17(10) **(1979),** 1098-1105.

[6] E. Robin James J. Appl. Phys. 49(10) **(1978)**, 5306-5310.

[7] S. M. Liang, Journal of Mechanics, vol. 25, No.3, Sept**.(2009).**

[8] S. Messer, F. D. Witherspoon, and M. Phillips: Hyper V Technologies, Inc. Chantilly, VA 20151: 1-24, **(2008).**

[9] H. Bassam: Dr. Thesis, Faculty of Science University of Baghdad, Baghdad, IRAQ **(1999).**

[10] L. I. Sedov: Similarity and dimensional methods in mechanics, (Academic Press, New York, **(1959).**